Diffusive dynamics in systems with translational symmetry:
A one-dimensional-map model

Mark Schell, Simon Fraser, and Raymond Kapral
Department of Chemistry, University of Toronto, Toronto, Ontario M5S 1A1, Canada
(Received 11 March 1982)

A one-dimensional, one-parameter-map model for dissipative systems with translational symmetry is studied. The map possesses confined periodic and chaotic solutions which form an infinite array on the real line, periodic or chaotic running solutions which propagate coherently to the left or right, and a variety of diffusive motions where iterates wander over the entire interval like a random walk. The onset of diffusion in various regions of parameter space is studied in detail and simple dynamical models for the behavior of the diffusion coefficient near bifurcation points are constructed.

I. INTRODUCTION

Far-from-equilibrium, nonlinear, dissipative systems display a rich structure of periodic and chaotic states. If such systems also possess translational symmetry new types of behavior are possible: There exist periodic and chaotic running solutions as well as diffusionlike motions. Likely candidates for such behavior are systems in which the underlying potential is periodic, and examples which have been recently studied include a driven superionic conductor[1] and a Josephson oscillator in the presence of microwave radiation.[2] Typically the equation of motion takes the form

$$\ddot{q} = -\dot{q}/\tau + a\sin 2\pi q + \mu\cos\omega t , \qquad (1.1)$$

where q denotes the ion position or superconductor phase. The first term on the right-hand side accounts for the dissipation, with τ the relaxation time, and the last term is the external force, which drives the system out of equilibrium. One may also consider the case of a parametrically driven oscillator[3]

$$\ddot{q} = -\dot{q}/\tau + (a + \mu\cos\omega t)\sin 2\pi q . \qquad (1.2)$$

Clearly these equations possess translational symmetry.

The multidimensional nature of the parameter space leads to a fairly elaborate pattern of bifurcations for these systems, but generally a number of distinctive processes are observed. For certain parameter values solutions are confined to a specified q interval (dependent on initial conditions) and do not cover the entire configuration space. These confined solutions may be either periodic or chaotic. Another type of motion corresponds to running solutions in which the particle coherently hops from one well to another in the periodic potential[2–4]; again such motion may be periodic or chaotic. The dominant type of motion is diffusion where the trajectory wanders in a random walklike fashion over the infinite interval. A common feature of these systems is the occurrence of broken symmetry, multistability, and hysteresis. The running solutions obviously possess broken-symmetry, running either to the right or left, also orbit-doubling bifurcations occur where an orbit splits to give two new orbits rather than one subharmonic orbit with twice the period.

In this article we attempt to provide a description of some aspects of the behavior of such systems. However, we do not study the differential equations of motion, but instead consider a simple, one-parameter, one-dimensional map which, by construction, has translational symmetry. This map model possesses all of the different types of solution referred to above, and, because of its simplicity, permits a detailed study of the pattern of bifurcations and the mechanisms by which they arise.

In Sec. II we describe the map and give an overview of the bifurcation structure as the map parameter is varied. Sections II and III are devoted to an analysis of the onset of diffusion. In Sec. III we discuss the mechanisms which operate when diffusive motion occurs, and in Sec. IV we construct models for the diffusion coefficient, which characterizes such random motion in various regions of parameter space. Section V contains a discussion of some aspects of the results.

II. CLIMBING-SINE MAP

Many features characteristic of nonlinear dissipative systems which possess translational symmetry are also exhibited by a simple "climbing-sine" map,

$$x_{t+1} = x_t + \lambda \sin 2\pi x_t \equiv S(x_t; \lambda) , \tag{2.1}$$

where λ is a parameter $-\infty < \lambda < +\infty$. However, only either positive or negative λ need be considered for the following reason: From Eq. (2.1) $\lambda = 0$ corresponds to a continuous symmetry of the system where every point x is fixed. For $\lambda < 0$ the equation of motion (2.1) becomes

$$x_{t+1} = x_t - |\lambda| \sin 2\pi x_t \tag{2.2}$$

or

$$x_{t+1} + \tfrac{1}{2} = x_t + \tfrac{1}{2} + |\lambda| \sin 2\pi (x_t + \tfrac{1}{2}) ,$$

so that in the plane $\Sigma = \{\lambda\} \times \{x\}$ the solution structure (stable periodic or chaotic orbits, etc.) for $\lambda < 0$ is a mirror image in the line $\lambda = 0$ of the solutions for $\lambda > 0$, but shifted by half a unit; on either side of $\lambda = 0$ the continuous symmetry is broken. The translational symmetry of S also implies that if $\{x_0, x_1, \ldots, x_r, \ldots\}$ is a trajectory then so are $\{x_0 + k, x_1 + k, \ldots, x_r + k, \ldots\}$ and $\{k' - x_0, k' - x_1, \ldots, k' - x_r, \ldots\}$ for all integers k and k' and it is useful throughout the discussion to think of sets of solutions being generated by such translations.

While discussing some properties of the differential flows in the Introduction we noted the existence of confined, running, and diffusive solutions. Similar types of behavior also exist for the map, this motion being characteristic at a particular value of λ. Operationally these classes of trajectories can be distinguished by the asymptotic properties of their first two moments, and in describing them we assume sufficient time has elapsed for transients to disappear. Confined solutions may be periodic or chaotic and eventually all their iterates lie within some finite interval (a,b); such orbits have finite "diameter" and asymptotically constant mean and dispersion. Running solutions, however, show, on average, a linear progress to the left or right with time. This motion may not be monotone but backtrack regularly; we shall consider only the simplest case without such reversals. The antisymmetric form of the map S [Eq. (2.1)] indicates that running solutions must come in pairs which, taken together, restore the overall dynamical symmetry. These solutions may be periodic or chaotic but are dispersionless: They have an asymptotically finite second

moment because any connected ensemble of points running to the left or right will migrate without spreading. Finally there exists a variety of diffusive solutions which behave like Markovian random walks. Although some of these solutions show initial persistence, i.e., a slowly decaying first moment, they have a vanishing asymptotic first moment and a growing second moment that shows a Gaussian-type increase at long times.

In the rest of this section we use the properties of simple periodic solutions and running solutions to illustrate some important dynamical features of the dispersionless solutions of S. Throughout this analysis it is convenient to divide the real line into a lattice of cells with the periodicity of S: The nth cell is the interval $[n-1, n)$ for integer n. For $\lambda > 0$ the cell boundaries $x = n$ are unstable fixed points and $x = n - \tfrac{1}{2}$, the cell midpoints, stable period 1 for small λ. For $\lambda < 0$ the stability of these two sets is reversed as indicated earlier; this broken symmetry is shown in Fig. 1. The way the stable period-1 solutions approach the line $\lambda = 0$ is reminiscent of the behavior of the residual magnetization of a fer-
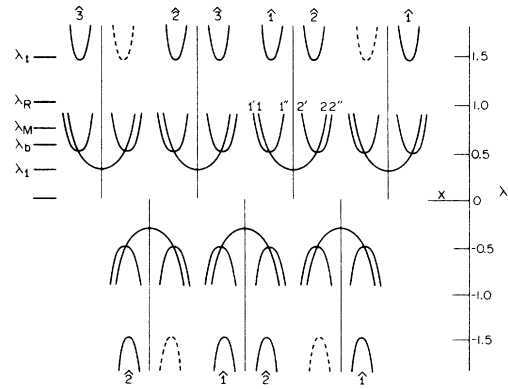
FIG. 1. Periodic solutions of S are shown. Vertical lines at equal intervals are period-1 solutions, stable at $\lambda = 0$ and becoming unstable at $|\lambda| = \lambda_1 = 1/\pi$. Note the half-integer shifts between the upper- and lower-λ half-planes. Period 1 subharmonically bifurcates into symmetric period 2, shown as (1,2) for one solution. At $\lambda = \tfrac{1}{2}$, (1,2) bifurcates to two asymmetric period 2's (1',2') and (1",2"). At $\lambda_b = 0.5483$ these bifurcate to two period 4's (not shown). Although truncated at $\lambda = 0.9$ such solutions persist for all larger λ values. $\lambda_M = 0.7326$ is the band-merging (migration) transition; $\lambda_R = 1$ is the transition to running solutions. $\lambda_t = 1.4653$ is the first tangent bifurcation to symmetric period 2, paired $(\hat{1},\hat{1})$, $(\hat{2},\hat{2})$, etc. Dashed curves have no mates in the Figure. For each such pair the outside is initially stable and the inside unstable. $\lambda = 1.5$ is the orbit-doubling bifurcation for these period 2's. Note that narrowing windows, e.g., $\lambda_1 - \tfrac{1}{2}$ vs $\lambda_t - \tfrac{3}{2}$ with increasing λ.

romagnet. Period 1 is stable for $0 \le \lambda \le 1/\pi$ and superstable at $\lambda = 1/2\pi$. For all points $x = n$ or $n - \frac{1}{2}$ (at any λ) $d^2S/dx^2 = 0$ so that covergence to superstable period 1 is exceptionally fast.

The period-2 fixed points can be found, as usual, from the second power of the map

$$x = S^{(2)}(x;\lambda) \equiv S(S(x;\lambda);\lambda) \qquad (2.3)$$

or explicitly

$$\sin\pi(2x + \lambda \sin 2\pi x)\cos(\pi\lambda \sin 2\pi x) = 0 . \qquad (2.4)$$

The two factors in Eq. (2.4) correspond to distinct types of period 2. From the first factor we obtain the equation

$$2x + \lambda \sin 2\pi x = n \quad (\text{integer } n) \qquad (2.5)$$

or

$$S(x;\lambda) = -x + n .$$

This latter form is especially convenient for graphical construction of the fixed points since they just correspond to the intersections of the family of straight lines $y = -x + n$ with the map function $S(x;\lambda)$. Equation (2.5) corresponds to symmetric[5] period 2 whose components are equidistant from the point $n/2$, a cell midpoint or boundary; their diameter $|x - S(x;\lambda)|$ is not greater than λ.

Similarly the second factor in Eq. (2.4) yields

$$\lambda \sin 2\pi x = \pm(m + \frac{1}{2}) \quad (m \text{ non-negative}) .$$
$$(2.6)$$

The orbits corresponding to Eq. (2.6) are unsymmetrical (with respect to either cell midpoints or boundaries) but come in conjugate pairs: indeed these pairs are born out of the symmetrical solutions of Eq. (2.5). In contrast to integer n in Eq. (2.5), m (or λ) in Eq. (2.6) determines the diameter of the orbit, not its position, since x appears only as an argument of a periodic function.

We now consider the configuration of period-2 solutions in the Σ plane: For λ smaller than some critical value[6] $\lambda_M \simeq \frac{3}{4}$ each cell is mapped into itself under S and trajectories cannot migrate on the lattice. Corresponding to this strictly confined dynamics for small λ we observe in Fig. 1 that the symmetric period-2's lying closest to the line $\lambda = 0$ arise from the stable period-1 solutions by subharmonic bifurcation[7,8] at $\lambda = 1/\pi$. The components of these period 2's separate as λ increases, first going through double superstability and reaching marginal stability at $\lambda = \frac{1}{2}$. At this point, where the solutions of Eqs. (2.5) and (2.6) coincide, period 2

splits by an orbit-doubling bifurcation into two conjugate, stable asymmetric period 2's. These orbits and their basins are interleaved. The symmetric period-2 bifurcations can be predicted from the derivative of $S^{(2)}$ which is given by

$$S^{(2)'} = (1 + 2\pi\lambda \cos 2\pi x)$$
$$\times [1 + 2\pi\lambda \cos 2\pi(x + \lambda \sin 2\pi x)] . \quad (2.7)$$

Using Eq. (2.5) we obtain

$$S^{(2)'} = (1 + 2\pi\lambda \cos 2\pi x)^2 , \qquad (2.8)$$

which is always positive. The conditions for marginal stability of symmetric period 2 are that $S^{(2)'} = 1$ and Eq. (2.5) be satisfied. This is true for $x = n - \frac{1}{2}$ at $\lambda = 1/\pi$ and for $x = n + \frac{1}{4}$ or $n + \frac{3}{4}$ at $\lambda = \frac{1}{2}$. May[9] has described precisely this phenomenon for the antisymmetric cubic map. Correspondingly up to $\lambda = \lambda_M$ the bifurcations within each cell are expected to follow those of the cubic map, where each pair of basins contains identical subharmonic cascades into confined chaos, tangent bifurcations,[7] etc., until eventually the symmetry of the solution is restored and at $\lambda = \lambda_M$ there is a continuous invariant density whose support is the entire cell width. For $\lambda > \lambda_M$ trajectories may wander between cells and there is a change in the dynamical origin of symmetrical period 2. Period 1 is unstable at these larger λ values so that period 2 cannot appear by a local subharmonic process; instead the form of Eq. (2.5) implies that symmetric period 2 arises by tangent bifurcation out of (diffusive) chaos. The orbit components are in this case well separated and, as usual, appear in stable and unstable pairs. The lowest-lying period-2 tangent bifurcation, shown in the Σ plane in Fig. 1, occurs at $\lambda_t = 1.465\,288\,265\,01$. Since the stable orbit components occur at unit intervals and the diameter of the orbit is nearly λ, these symmetric period 2's necessarily interlace. As λ increases further this symmetric solution undergoes an orbit-doubling bifurcation at $\lambda = 1.5$. The asymmetric period-2 orbits then undergo subharmonic cascade into chaos, etc., which breaks down into diffusion since the orbits are no longer confined within single cells. Orbit doubling from symmetric, tangent period 2 occurs at every (larger) half-integer λ value, the resulting asymmetric period 2's being followed by subharmonic cascade; this symmetry-breaking bifurcation connects the sets of solutions of the two factors of Eq. (2.3). The criteria $S^{(2)'} = 1$ and $S^{(2)} - x = 0$ also hold for bifurcation of these "tangent" symmetric period 2's and although the period-doubling bifurcation can always be found very easily the tangent

bifurcation itself can only be determined from a transcendental equation. For the components this is

$$\tan 2\pi x - 2\pi x + \pi n = 0 \tag{2.9}$$

and λ_t is given by (see Table I for a tabulation of λ_t values)

$$\lambda_t = -\frac{1}{\pi \cos 2\pi x} , \tag{2.10}$$

where n has the value appearing in Eq. (2.5). From Eq. (2.10) λ_t diverges as x tends to $n + \frac{1}{4}$ or $n + \frac{3}{4}$, which alternatively stated means we observe decreasing stability windows with increasing λ, the orbit components converging to the asymptotic positions of the map extrema.

The two sets of asymmetric period 2's that arise from the symmetric tangent orbits are

$$x_1 = n + \frac{1}{2\pi} \arcsin \left[\frac{2m+1}{2\lambda} \right]$$

$$(n - \tfrac{1}{4} \leq x \leq n + \tfrac{1}{4})$$

$$x_2 = n + \frac{2m+1}{2} + \frac{1}{2\pi} \arcsin \left[\frac{2m+1}{2\lambda} \right]$$

$$(m + n + \tfrac{1}{4} \leq x \leq m + n + \tfrac{3}{4}) \tag{2.11}$$

and

$$x_1' = \frac{2n+1}{2} - \frac{1}{2\pi} \arcsin \left[\frac{2m+1}{2\lambda} \right]$$

$$(n + \tfrac{1}{4} \leq x \leq n + \tfrac{3}{4})$$

$$x_2' = m + n + 1 - \frac{1}{2\pi} \arcsin \left[\frac{2m+1}{2\lambda} \right]$$

$$(m + n + \tfrac{3}{4} \leq x \leq m + n + \tfrac{5}{4}) \tag{2.12}$$

where λ must satisfy the condition $(2m+1)/2\lambda \leq 1$. These solutions are stable for

$$m + \tfrac{1}{2} \leq \lambda \leq [(2\pi^2)^{-1} + (m + \tfrac{1}{2})^2]^{1/2} . \tag{2.13}$$

Clearly

$$x_1 + x_2' = x_2 + x_1' = 2n + m + 1 . \tag{2.14}$$

We now summarize the properties of the simplest (monotone) running solutions which can only occur above the threshold $\lambda = \lambda_M$; like confined solutions for $\lambda > \lambda_M$ these may break down into diffusive motion. They satisfy the condition

$$x_{t+1}^{(\pm)} = x_t^{(\pm)} \pm m \quad (m \text{ a positive integer}) \tag{2.15}$$

where the $\pm$ signs refer to iterates running to the right or left. The solutions of Eq. (2.1) that satisfy this condition are obtained from

$$\pm m = \lambda \sin 2\pi x^{(\pm)} . \tag{2.16}$$

The explicit solutions are

$$x^{(\pm)} = n + \tfrac{1}{2} \mp \frac{1}{2\pi} \arcsin \left[\frac{m}{\lambda} \right]$$

$$(n + \tfrac{1}{4} \leq x \leq n + \tfrac{3}{4}) . \tag{2.17}$$

These solutions are stable for

$$m \leq \lambda \leq (\pi^{-2} + m^2)^{1/2} \tag{2.18}$$

with superstability occurring at $\lambda = [(4\pi^2)^{-1} + m^2]^{1/2}$. When λ is increased beyond $(\pi^{-2} + m^2)^{1/2}$ in each integer interval of λ this "period-1" running solution bifurcates to a period-2 running solution and a subharmonic cascade takes place culminating in a chaotic running solution. There are actually large numbers of coexisting running solutions. If we have a running solution with period 2^n then there are, in general, $m 2^{n+1}$ separate attracting solutions; each point on an attracting orbit satisfies the condition

$$S^{(2^n)}(x^{(\pm)}; \lambda) = x^{(\pm)} \pm m 2^n . \tag{2.19}$$
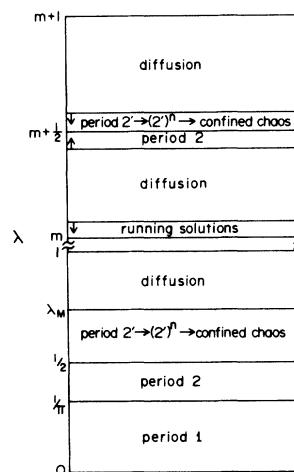
FIG. 2. Diagram depicts some of the major bifurcation sequences for the climbing-sine map. Regions labeled period 2 correspond to symmetric period-2 orbits, while period 2' refers to broken-symmetry period-2 orbits. The regions containing the subharmonic bifurcations and subsequent confined chaos arising out of period 2' are not drawn to scale. The vertical arrows in the upper portion of the figure indicate the directions in which the boundaries move as m increases. The large diffusion regions are punctuated by small windows of other types of periodic and nondiffusive behavior.

TABLE I. Tabulation of transition points corresponding to the onset of diffusive motion as a function of m. λ_M, value of λ at which the probability of jumping from cell n to cell $n\pm(m+1)$ within one iteration becomes finite; λ_t, tangent bifurcation from diffusion to confined period 2; λ_{CR}, breakdown of chaotic running bands into diffusion; λ_{Ct}, breakdown of confined two-banded chaos into diffusion. Running solutions are born out of chaos by a tangent mechanism at $\lambda_R = m$. The correspondence between λ_t and m is achieved by restricting x in Eq. (2.9) to $\frac{1}{4} < x < \frac{1}{2}$ and setting $n = m + 1$. It is interesting to note that $2\lambda_M = \lambda_t$ for those λ_t whose integer value is odd. This follows from the fact that Eq. (3.2) and the defining equation for M, $\cos 2\pi M = 1/2\pi\lambda_M$, are equivalent to Eqs. (2.9) and (2.10) if n and λ_t are replaced by $2(m+1)$ and $2\lambda_M$, respectively. An analogous relation exists between those λ_t whose integer value is even and a set of transition values λ'_M which correspond to the first occurrence of direct mappings from cell n to beyond the midpoint of cell $n\pm(m+1)$. The relevant equation is $S(M;\lambda'_M) = S(-M+m+3;\lambda'_M) = m + \frac{3}{2}$, where M is the maximum in cell one.

m	λ_M	λ_t	λ_{CR}	λ_{Ct}
0	0.732 644 1325			
1	1.742 727 5076	1.465 288 2650	1.108 230 0133	1.541 891 9939
2	2.745 385 4573	2.479 540 3563	2.056 206 9659	2.525 257 9399
3	3.746 619 0709	3.485 455 0151	3.037 758 3170	3.518 066 4833
4	4.747 331 9046	4.488 709 0356	4.028 395 9089	4.514 059 8360
5	5.747 796 3803	5.490 770 9145	5.022 745 5687	5.511 506 8851
6	6.748 123 0729	6.492 195 1287	6.018 967 7561	6.509 738 2458
7	7.748 365 3851	7.493 238 1418	7.016 264 8727	7.508 440 7121
8	8.748 552 2751	8.494 035 0466	8.014 235 6293	8.507 448 2178
9	9.748 700 8085	9.494 663 8091	9.012 656 2511	9.506 664 5281
10	10.748 821 6960	10.495 172 5924	10.011 392 1453	10.506 030 0307

The subharmonic cascade of the confined solutions described earlier as well as that for the running solutions satisfy Feigenbaum's scaling.[8,10]

In this section we discussed period-1 and -2 solutions: In the parameter regime $\lambda \leq \lambda_M$ escape from any cell is impossible; the solution structure for S is a periodic analog of the bound solutions for the antisymmetric cubic map; just above this λ value, migration between cells ensues. At a series of larger λ values, period 2 arises out of diffusive chaos by tangent bifurcation and undergoes orbit doubling at half-integer λ values followed by a subharmonic cascade into conjugate pairs of chaotic bands, etc., which then break down again into diffusive chaos. The other important nondispersive motions are the running solutions. Their bifurcation history with increasing λ follows the usual route of subharmonic cascade into chaotic running bands with eventual reemergence of diffusive behavior. Broken symmetry is an intrinsic feature of these trajectories. The cycles and sequences of these phases are summarized in Fig. 2 which displays only the dominant structure discussed above. From Eqs. (2.13) and (2.18) which refer to such confined and running solutions we infer that the width of the windows is $O(m^{-1})$ for large m. In other words we expect the bandwidth of a hierarchy of solutions to decrease as

λ^{-1}. Other, finer bifurcation histories are embedded in $\{\lambda\}$. We now turn to a detailed description of diffusion under S and its connection with dispersionless behavior.

III. MECHANISMS FOR THE ONSET OF DIFFUSIVE MOTION

The onset of diffusive motion occurs in several characteristic ways for this map. Diffusive orbits may arise from both confined chaotic and running chaotic solutions; also, diffusive orbits may bifurcate to give periodic running or confined solutions. Below we describe the mechanisms by which these transitions take place and give examples.

A. Chaotic-band merging

The first transition into diffusive motion occurs at $\lambda = \lambda_M = 0.732\,644\,1325\ldots$ and involves the merging of the array chaotic bands that were confined within separate unit cells for $\lambda < \lambda_M$. The band-merging mechanism can be discussed in more detail by referring to Fig. 3, which shows the map in the first cell for $\lambda < \lambda_M$. From the figure it is clear that the maximum M is mapped into B while
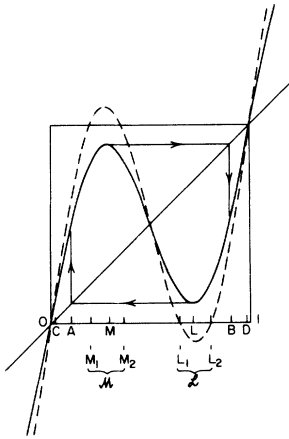
FIG. 3. Solid curve is the graph of $S(x;\lambda)$ in the first cell for $\lambda \lesssim \lambda_M$. Iterates are confined to the interval AB, where A and B are the images of the minimum L and maximum M, respectively. Dashed curve depicts S for $\lambda > \lambda_M$. Points in the intervals $\mathscr{M}$ and $\mathscr{L}$ escape to neighboring cells.

the minimum L is mapped into A; both A and B are mapped into the interior of AB. Furthermore, the intervals $0A$ and $B1$ are eventually mapped into AB; since C and D are the preimages of A and B, respec-
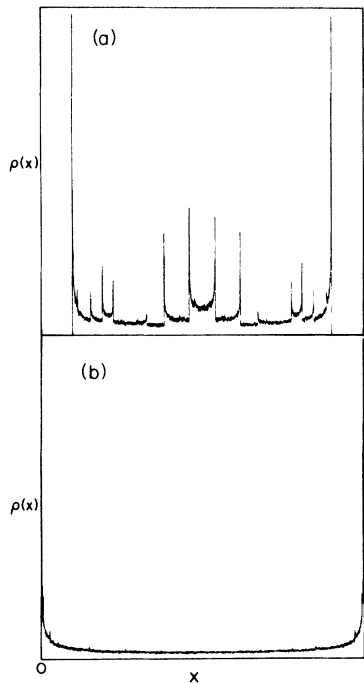
FIG. 4. Plots of the invariant density $\rho(x)$ illustrating chaotic-band merging. (a) $\lambda = 0.6328 < \lambda_M$; a chaotic band in cell one. Identical bands exist in other cells. (b) $\lambda = 0.7328 \gtrsim \lambda_M$; the bands which were confined to cells have merged.

tively, CA and BD are mapped directly into AB while points in $0C$ and $D1$ require more than one iteration to reach this interval. However, it is generally observed for λ close to λ_M that every open neighborhood of AB is visited by almost all trajectories starting in AB, so that AB supports a continuous invariant density. This is the usual way in which banded chaotic regions are formed[8,11,12], and in the present case one has an infinite number of such disjoint bands, one in each cell. The stroboscopic density [density for x (mod 1)] for this case is shown in Fig. 4(a).

As λ is increased the value of the map at the maximum in cell one becomes equal to unity (of course, simultaneously the map at the minimum becomes equal to zero and maxima and minima in other cells achieve integer values) and escape to neighboring cells is possible. At this transition value of λ ($=\lambda_M$), B, the image of the maximum, coincides with the unstable fixed point $x = 1$ while A coincides with $x = 0$. Thus λ_M is determined by the condition

$$S(M;\lambda_M) = S(-M+2;\lambda_M) = 1 . \qquad (3.1)$$

The second equality follows from the fact that at λ_M the minimum in cell two, which is located at $-M+2$, is also mapped onto one. The density for a value of $\lambda \gtrsim \lambda_M$ is shown in Fig. 4(b). This cellwise band-merging process is analogous to that described by other workers for band merging in the quadratic map.[11-14] It is clear that a condition such as this will apply whenever the maxima and minima of S pass through an integer value; thus one may write the more general relation

$$S(M;\lambda_M) = S(-M+m+2;\lambda_M) = m+1 . \qquad (3.2)$$

However, while the value of λ_M obtained from Eq. (3.1) corresponds to a transition to diffusive motion, the transition values λ_M obtained from Eq. (3.2) for $m \neq 0$ lie in a λ region for which the motion is already diffusive: these values of λ_M correspond to the first occurrence of direct mappings from cell n to cell $n \pm (m+1)$. The values of λ_M are given in Table I for several values of m.

B. Tangent mechanism

The large diffusive region which begins at λ_M terminates in a period-1 running solution at $\lambda = 1$. (As noted earlier, this region is punctuated by small windows of various types of nondiffusive orbits. We shall not discuss such fine structure here but in-
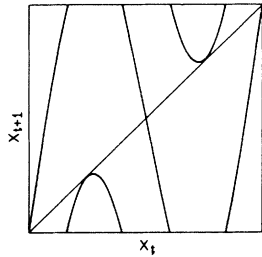
FIG. 5. Map iterates (mod 1) for $\lambda \leq 1$. Running solutions arise by a tangent mechanism when the map (mod 1) touches and then crosses the bisectrix.

stead focus only on the major transitions.) The running solution is born out of the diffusive solution by a tangent bifurcation mechanism. This is most easily seen in the mod-1 representation of the dynamics shown in Fig. 5, where map iterates (mod 1) are plotted for a value of λ somewhat less than unity. It can be seen that the map function approaches and finally touches the bisectrix; the slope of the map for $\lambda = 1$ at these touching points has the value $+1$ characteristic of a tangent bifurcation process. Since a tangent mechanism is operative one expects that the diffusive motion will exhibit intermittency.[15-19] For values of λ slightly smaller than unity iterates (mod 1) consist of small steps through the channels formed by the bisectrix and the map function (mod 1) near the maximum and minimum. Close to bifurcation the widths of the channels are small, leading to a large number of steps, and since the length of the channel is also small we have a large number of nearly periodic iterates. In the actual dynamics, motion through the channel associated with the map maxima consists of iterates running to the right with a step length of approximately one cell, while the left-running solutions takes place in the channel associated with the map minima. Outside these channels, the motion is apparently irregular and diffusionlike. Hence, the dynamics exhibit the features characteristic of intermittency: long, nearly periodic runs to the left or right interspersed with irregular, diffusive motion. Provided one works in a mod-1 representation a model for the evolution can be constructed which parallels that for the chaos to period-3 transition in the logistic equation.

As in the case of the logistic equation the dynamics is most conveniently discussed by partitioning the unit interval into basins and watersheds [cf. Fig. 6(a)].[16] A basin $\mathscr{B}$ is a small region of the unit interval in which the motion of the map iterates is regular and nearly periodic. In the present case we have two basins chosen symmetrically about the
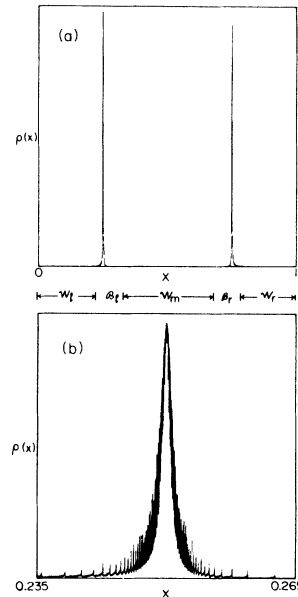
FIG. 6. (a) Invariant density (mod 1) in the diffusive region $\lambda \leq 1$ which precedes the appearance of running solutions. Inset shows the partitioning into watersheds and basins. (b) A magnified picture of the left resonance spike which shows the decoration by spires arising from the square-root singularity in the functional map.

map maximum and minimum (mod 1), which contain the channels described above. The left basin $\mathscr{B}_l$ is associated with iterates that run to the right but the local drift from the initial value (iterate mod 1) is to the left, i.e., while the iterates consist of steps of approximately unit length to the right, they become shorter as they progress through the channel. Similarly the right basin $\mathscr{B}_r$ corresponds to iterates running to the left with local drift to the right. The remainder of the unit interval consists of watersheds where the motion is chaotic. The middle watershed $\mathscr{W}_m$ is located between $\mathscr{B}_l$ and $\mathscr{B}_r$ while the watersheds W_l and W_r lie to the left of $\mathscr{B}_l$ and to the right of $\mathscr{B}_r$, respectively. An analogous description holds near any integer value of λ except that at $\lambda = m$ the iterates are able to hop m cells at each step.

Because of the large number of steps in the basins the invariant density in the mod-1 representation is sharply peaked in these regions, as can be seen in Fig. 6(a), with only a small and roughly uniform density between the spikes. The local (mod-1) motion and invariant density within the basins can be described by a resonance[16] or continuum[15,17] model since the steps are small. Given the nature of the running solution in Eq. (2.15), the "fixed points" corresponding to these solutions are given

by Eq. (2.16). For λ less than m in each integer interval of λ there are (locally) no real stable solutions to this equation; there are, however, complex solutions $z^{\pm}$ which close to bifurcation are given by

$$z^{(\pm)} \equiv \xi_{r,l} \pm i\eta_R = \begin{cases} \frac{1}{4} \pm \frac{i}{\pi}(\epsilon/2m)^{1/2} , \\ \frac{3}{4} \pm \frac{i}{\pi}(\epsilon/2m)^{1/2} , \end{cases}$$ (3.3)

where $\epsilon = m - \lambda$. These complex fixed points govern the dynamics on the real line.

The invariant density within $\mathcal{B}_l$ or $\mathcal{B}_r$, ρ_l or ρ_r, respectively, can be obtained from a continuity equation supplemented with a source term[17]: Iterates which enter the watershed $\mathcal{W} = \mathcal{W}_l \cup \mathcal{W}_m \cup \mathcal{W}_r$ are strongly mixed and assumed to reenter a basin uniformly at a rate r per iteration. The continuity equation involves the velocities of the iterates (mod 1), which, near bifurcation, can be expressed in terms of the real and imaginary parts of the complex fixed points:

$$\dot{X}_{r,l} \equiv \Delta_{r,l} = C_{r,l}(X_{r,l}^2 + \eta_R^2) ,$$ (3.4)

where $X_{r,l} = x - \xi_{r,l}$ and $C_{r,l} = \mp 2m\pi^2 \equiv \mp C$. The invariant densites are thus given by the solutions of the continuity equation

$$\frac{d}{dX_{r,l}}[\Delta_{r,l}(X_{r,l})\rho_{r,l}(X_{r,l})] = r .$$ (3.5)

Very close to bifurcation the density in the basins is nearly Lorentzian in shape,[16]

$$\rho_{r,l}(x) = \frac{1}{2\pi} \frac{\eta_R}{(x - \xi_{r,l})^2 + \eta_R^2} ,$$ (3.6)

with centers at $\frac{1}{4}$ and $\frac{3}{4}$ with halfwidths η_R. These features are confirmed by the density in Fig. 6. We also note that the uniform reentry of iterates into the basins, in conjunction with the local flow of iterates within a basin, leads to the skewing of the spikes to the left for ρ_l and to the right for ρ_r. The magnified left resonance spike [Fig. 6(b)] also exhibits the decoration by small spires which arise from the square-root singularity in the functional mapping.[16]

The local continuum model of the map [Eq. (3.4)] can also be used to compute the probability distribution of runs of length t given a random entry into a basin. For a channel length of $2X_0$ the result is[17]

$$P(t) = \frac{a\eta^2}{2X_0}\{1 + \tan^2[\arctan(X_0/\eta) - C\eta t]\} ,$$ (3.7)

with $a = 1$ and $\eta = \eta_R$. The maximum length of a run before the basin boundary is crossed and entry into the watershed occurs is $t_{max} = (2/C\eta) \times \arctan(X_0/\eta)$, while the average length of a run is $\langle t \rangle = (C\eta)^{-1} \arctan(X_0/\eta)$. We shall have occasion to use these results in Sec. IV where the diffusion coefficients are discussed.

The tangent mechanism is also operative for the transition from diffusion to confined period 2 that occurs for values of λ somewhat less than $m + \frac{1}{2}$; the first transition occurs at $\lambda_t = 1.465\,288\,2650$. The second power of the map is plotted in Fig. 7 and shows the maxima and minima that approach the bisectrix as the bifurcation point is reached. The analysis is similar to that for the logistic equation near period 3 except that now one must work with the fixed-point equation for the second power of the map and deal with the infinite interval since the period-2 orbits are interlaced as discussed in Sec. II.

In order to partition the infinite interval into basins and watersheds, consider the graph of the
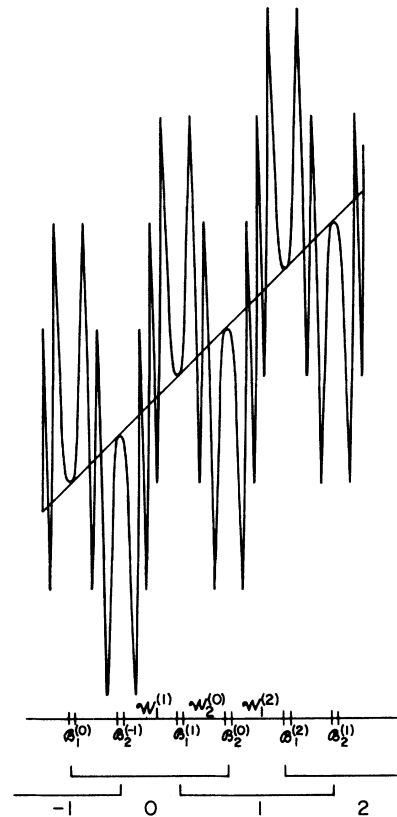
FIG. 7. Plot of $S^{(2)}(x;\lambda)$ for $\lambda = 1.465 \simeq \lambda_t$ illustrating the appearances of period 2 by a tangent mechanism. Inset shows the partition of the (infinite) interval into basins and watersheds.

second power of the map in Fig. 7. We designate the two basins associated with an almost resonant period-2 orbit type one or type two depending on whether $S^{(2)}(x;\lambda)$ approaches the bisectrix from above or below, respectively. The orbits are numbered according to the scheme in Fig. 7. Thus, basins will be denoted by $\mathscr{B}_{1,2}^{(i)}$, where i labels the orbit. Note that the ith orbit has fixed points in cells i and $i+m$. From the figure one can see that the basins are interleaved in the sequence $\{\mathscr{B}_1^{(i)}, \mathscr{B}_2^{(i-1)}, \mathscr{B}_1^{(i+1)}, \mathscr{B}_2^{(i)}\}$. Watersheds lie in between these basins. Denote the watershed that immediately precedes the basin $\mathscr{B}_k^{(i)}$ by $\mathscr{W}_k^{(i)}$. It can be seen that $\mu(\mathscr{W}_1^{(i)}) > \mu(\mathscr{W}_2^{(j)})$. The full watershed is $\bigcup_{i,k}\mathscr{W}_k^{(i)} = \mathscr{W}$. Motion in $\mathscr{W}$ is chaotic and diffusive; when an iterate enters a basin it is trapped for long periods of time in the period-2 resonance.

For the application of the resonance model to this case we notice that Eq. (2.3) fails to have real solutions locally for values of $\lambda \lesssim \lambda_t$ but does possess solutions in the complex plane, which lie close to the real axis;

$$z_i = S^{(2)}(z_i;\lambda) \quad (i=1,2) \tag{3.8}$$

and near bifurcation

$$z_i = \xi_i^B \pm \frac{i}{\pi}\left[\frac{\epsilon}{2\lambda_t}\right]^{1/2} \equiv \xi_i^B \pm i\eta_t , \tag{3.9}$$

where ξ_i^B is the solution to Eq. (2.5) at bifurcation and $\epsilon = \lambda_t - \lambda$. The motion within each basin is again well approximated by a continuum model and the stroboscopic velocity can be obtained from the expansion of $S^{(2)}(x;\lambda)$ near bifurcation:

$$\dot{X}_{1,2} = \Delta_{1,2}^{(2)}(x;\lambda) = C_{1,2}(X_{1,2}^2 + \eta_t^2) ,$$

with $X_i = x - \xi_i^B$ and

$$C \equiv C_1 = (2\pi)^2 \lambda_t \sin 2\pi \xi_1^B = -C_2 .$$

The probability of a run of length t in a basin is given by Eq. (3.7) with $a = C/2\pi^2\lambda_t$ and $\eta = \eta_t$ in Eq. (3.9). The model predicts that the invariant density in a cell will consist of two nearly Lorentzian resonance spikes with a small uniform density in the watershed. From an examination of Fig. 7 it is clear that the stroboscopic flow in a type-1 basin is from left to right while it is from right to left in a type-2 basin. Thus both resonance spikes in a cell will be skewed toward the center of the cell. All of these features are confirmed by the density shown in Fig. 8.

While both of these transitions can be described by a tangent mechanism, the underlying physical
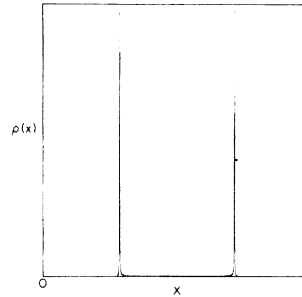
FIG. 8. Invariant density in cell one for $\lambda = 1.465\,280\,26 \lesssim \lambda_t$. Note that the two spikes in cell 1 are associated with different incipient period-2 orbits.

situation is quite different in each case. In the transition from diffusion to running solutions the coherence length of the iterates diverges as λ_R is approached; it is only in the mod-1 representation that the steps are small and a continuum description applies. One expects the diffusion coefficient to diverge. This diffusion is dominated by the contribution from $\mathscr{B}$, the contribution from $\mathscr{W}$ being negligible. On the other hand, for the transition from diffusion to confined period 2 one again observes intermittent behavior in the time series but now iterates are confined for long periods of time. One expects the diffusion coefficient to vanish at λ_t. In this case $\mathscr{B}$ contributes nothing to the diffusion coefficient; only the motion in $\mathscr{W}$ is important. These features will be discussed in detail in the next section.

C. Chaotic-band breakdown

The running solutions which are born at $\lambda_R = m$ subharmonically bifurcate and ultimately give rise to chaotic running solutions; as λ is increased further these solutions break down and a diffusive state appears. The mechanism for this transition can be described by referring to Fig. 9. Recall that the running solutions have broken symmetry, streaming either to the right or left. Consider the maximum of the map in cell one, which occurs at M and belongs to a chaotic solution running to the right. The maximum is mapped into $A+m$, $A+m = S(M;\lambda)$; A is mapped into $B+m$, $B+m = S(A;\lambda)$. The point E is also a preimage of $B+m$, $B+m = S(E;\lambda)$. Suppose that $E < B$; then (mod-1) points in the interval EB are mapped into the interior of BA. Similar considerations apply to the points L, A', B', and E' associated with the minimum (left-running solution). Points in the intervals OE, AA', $E'1$ are eventually mapped into BA
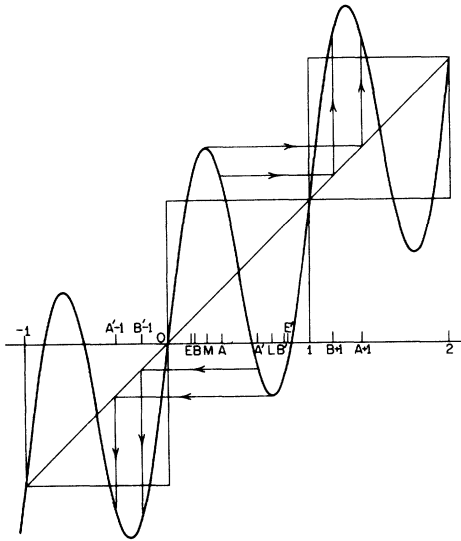
FIG. 9. Plot of $S(x;\lambda)$ in three cells showing the sequence of mappings which lead to the formation and breakdown of chaotic running bands.

or $A'B'$ giving rise to a chaotic band associated with a solution running either to the right or left depending on the initial condition. The density (mod 1) is shown in Fig. 10(a). As λ is increased and the map steepens, the point B (B') becomes equal to and then less (greater) than E (E'). When this occurs points in the intervals BE and $E'B'$ are mapped out
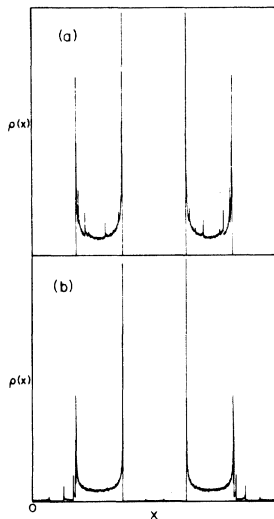
FIG. 10. (a) Invariant density (mod 1) for $\lambda = 1.108 \lesssim \lambda_{CR}$. Both left- and right-running chaotic bands are shown. Given an initial x on (0,1) either a left- or right-running band will be generated. (b) Invariant density for $\lambda = 1.1085 \gtrsim \lambda_{CR}$; a small but finite density exists between the bands indicating chaotic-band breakdown.

of the BA and $A'B'$ intervals breaking down the chaotic running bands [see Fig. 10(b)]. Note the existence of two-banded chaos corresponding to the appearance of both left- and right-running solutions and a small density between these chaotic bands.

The critical condition is clearly $E = B$ or $E' = B'$. Thus,

$$S^{(3)}(M;\lambda_{CR}) = S^{(2)}(M;\lambda_{CR}) + m .   (3.10)$$

The λ_{CR} values are given in Table I. This breakdown mechanism is similar to the 3 to 1 chaotic transition discussed by Chang and Wright.[12]

A somewhat more complicated version of this mechanism is applicable to the transition from confined chaotic solutions to diffusion. Recall (cf. Fig. 2) that broken-symmetry period-2 orbits appear at $\lambda = m + \frac{1}{2}$ and are followed by a subharmonic cascade, which results in a confined chaotic solution with a Cantor-set structure. As λ is increased this Cantor set undergoes a mirror sequence of band mergings and eventually forms a two-banded region with broken symmetry. A further increase in λ leads to a restoration of the map symmetry. It is from this symmetric, two-banded chaos that the transition to diffusion occurs. The transition takes place for λ values where the confined solutions are intertwined. Thus a chaotic band contained within an interval which includes the maximum in cell n is coupled to a chaotic band which includes the minimum in cell $n + m$.

To see how the bands originate consider the following sequence of mappings. Let M be a maximum of $S(x;\lambda)$ in cell one and L a minimum in cell $m + 1$, $L = -M + m + 1$. Then referring to Fig. 11(a), which corresponds to the case $m = 1$, we have

$$M \rightarrow A' \rightarrow B \rightarrow \text{int of } B'A'$$

and   (3.11)

$$L \rightarrow A \rightarrow B' \rightarrow \text{int of } AB .$$

Points outside of these bands are eventually mapped into them or into the other interlaced bands. In particular, if E is the preimage of B' and E' is the preimage of B, then the intervals BE and $E'B'$ are mapped into the interiors (int) of $B'A'$ and AB, respectively. As in the previous case, when λ is increased B and E $(B'$ and $E')$ coincide and then pass each other. In this case the intervals EB and $B'E'$ act as drains on the density in the banded chaotic regions. The situation shown in Fig. 11(b) results; one now sees the chaotic bands on (0,2) are connected by a small density between the bands. The con-
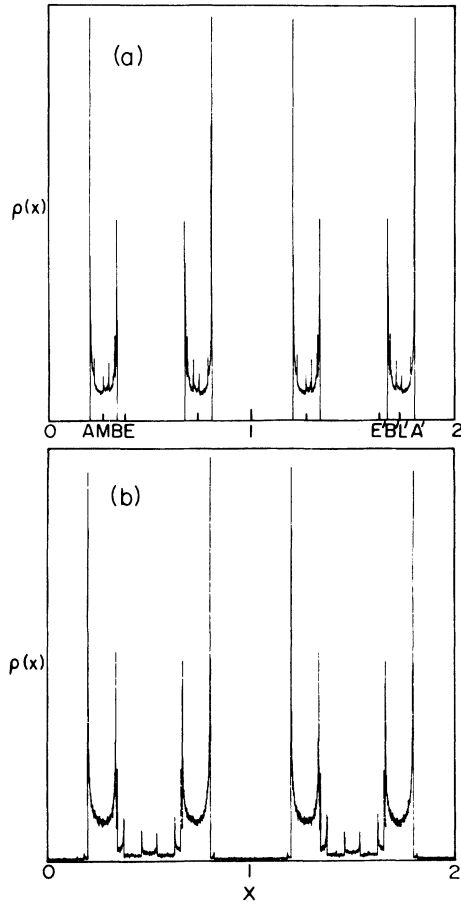
FIG. 11. (a) Invariant densities in two cells for $\lambda = 1.5416 \leq \lambda_{Ct}$. Chaotic band in cell 1 associated with the map maximum is coupled to that in cell 2 associated with the minimum. (b) Invariant density for $\lambda = 1.5428 \geq \lambda_{Ct}$ when the chaotic bands have broken down.

dition for a transition is again that the points E and B (or E' and B') coincide. Thus,

$$S^{(2)}(M;\lambda_{Ct}) = S^{(3)}(L;\lambda_{Ct})$$

$$= S^{(3)}(-M + m + 1;\lambda_{Ct}) . \quad (3.12)$$

The values of λ_{Ct} for several values of m are given in Table I.

We note again that while the above mechanisms are similar the underlying physical processes are quite different: one expects that the diffusion coefficient will diverge in the transition from diffusion to chaotic running solutions, and vanish for the transition from diffusion to confined chaotic solutions.

IV. DIFFUSION COEFFICIENTS

The nature of the diffusive state in the various regions of parameter space can be studied through an examination of the mean-square displacement of the map iterates and the associated diffusion coefficient, which is defined by the usual relation

$$D = \lim_{n \to \infty} \frac{\langle (x_n - x_0)^2 \rangle}{2n}$$

$$\equiv \lim_{n \to \infty} \frac{\langle (\Delta x_n)^2 \rangle}{2n} , \quad (4.1)$$

where x_n is the position at iterate n given the seed x_0. Note that x_0 determines x_n by iteration of the map. However, in the diffusive regime x_n is a "wild" function of x_0, which allows x_n to be treated as a random variable in the limit of large n. For such ill-conditioned motion one identifies the ensemble average with random sampling of x_0 over the invariant density (mod 1). The mean-square displacement was computed by averaging over an ensemble of 1000 points in the first cell distributed according to the invariant density and the diffusion coefficient was calculated from runs of 10 000 map iterates. These results indicate that near bifurcation the diffusion coefficient depends on the square root of the deviation of the map parameter from bifurcation. In this section we discuss the nature of the diffusive motion in more detail and present models for the diffusion coefficients in each of the regions, which show the origin of this square-root dependence.

A. Diffusion → confined chaos

From the discussion in Sec. III A it is clear that the transition from confined chaos to diffusive motion, which occurs at λ_M, arises by iterates "leaking" from small regions about the maximum M and minimum L of the map; points near M are mapped into the cell to the right while points near L are mapped to the left-hand cell (refer to the dashed curve in Fig. 3). The motion of iterates at bifurcation is chaotic and the invariant density in a cell closely corresponds to that for the cubic map,[11] $x_{t+1} = x_t(3 - 4x_t)^2$; $\rho(x) = [\pi \sqrt{x(1-x)}]^{-1}$ (cf. Fig. 4). Thus, with the assumption of chaotic motion of the iterates, just beyond bifurcation the probability of a step to the right or left will be proportional to the measure of the intervals (cf. Fig. 3) $\mathcal{M} = (M_1, M_2)$ and $\mathcal{L} = (L_1, L_2)$, $\mu(\mathcal{M}) = M_2 - M_1$ and $\mu(\mathcal{L}) = L_2 - L_1$, respectively: the measures of these intervals grow as $\epsilon^{1/2}$,

$$\mu(\mathcal{M}) = \mu(\mathcal{L}) = (2\epsilon/\lambda_M \pi^2)^{1/2} , \quad (4.2)$$

where $\epsilon = \lambda - \lambda_M$.

The model we adopt for the diffusive motion in

this region is an unrestricted random walk with probabilities p and q of taking steps to the right or left, respectively, given by

$$p = \int_{\mathcal{M}} \rho(x)dx = q = \int_{\mathcal{L}} \rho(x)dx , \qquad (4.3)$$

where the invariant density $\rho(x)$ is normalized to unity on the unit interval. The probability of an iterate remaining in the same cell is, of course, $r = 1 - (p + q) = 1 - 2p$. Given this model for the diffusive dynamics the diffusion coefficient is easily obtained from the known mean-square displacement[20] $\langle (\Delta x_n)^2 \rangle = [p + q - (p - q)^2]n$. Hence, near bifurcation D is given by

$$D = p \simeq \rho(M_B)(2\epsilon/\lambda_M \pi^2)^{1/2}$$
$$= 0.371\epsilon^{1/2} , \qquad (4.4)$$

where the last two lines follow from Eqs. (4.1) and (4.2) and the known values of M_B (the maximum at the bifurcation point, henceforth denoted by the subscript B) and λ_M, $M_B = 0.2848516736$ and $\lambda_M = 0.7326441325$. The numerical results given in Table II and displayed in Fig. 12 are in good agreement with the predictions of this model. The hopping which gives rise to diffusive motion is similar to the band-to-band hopping discussed by Shenker and Kadanoff.[21]

One additional feature of this transition should be noted. From Fig. 3 one can see that in a transition to a neighboring cell a parcel of probability fluid is mapped into an $O(\epsilon)$ region $[S(M;\lambda) - 1$ and $S(L;\lambda)$ are $O(\epsilon)$ near bifurcation] near the unstable fixed points at $x = 0$ and 1. Before such a parcel of probability fluid can be reemitted there must be time lapse $O(\ln\epsilon)$. This rather weak dependence on ϵ does not appear to vitiate the simple
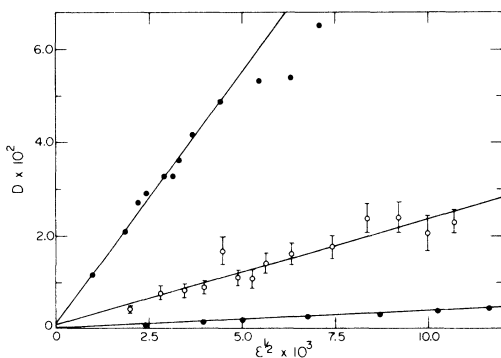
FIG. 12. Diffusion coefficient as a function of $\epsilon^{1/2}$. (lower) (●), chaotic-band-merging region; solid circles (upper) (●), confined period-2 region; open circles (○), chaotic period-2-band region. Error bars refer to ±1 standard deviation.

TABLE II. Diffusion coefficients near bifurcation.[a]

	Numerical estimate	Model
Diffusion → confined chaos	0.379	0.371
Diffusion → running solutions	0.348	0.354
Diffusion → chaotic running solutions	0.630	0.823
Diffusion → confined period 2	10.8	6.30
Diffusion → chaotic period 2	2.27	1.69

[a]Near bifurcation all diffusion coefficients have the form $D = d\epsilon^{\pm 1/2}$. The table lists the values of d for the various cases. The model calculations use the theoretical estimates of lifetimes, etc.

model of the diffusive motion and justifies the simple independent trial model for escape [Eq. (4.3)] where these memory effects are neglected. A further point is that a continuous invariant density implies positive Liapunov number for the motion and mixing within each cell before escape. This is compatible with an underlying assumption of statistical independence. In fact, using the equation $D = p$ and the numerically calculated values for p yields a good approximation for D throughout the interval $\lambda_M < \lambda < 1$ (excluding, of course, the neighborhoods of small windows containing nondiffusive solutions).

B. Diffusion → running solutions

At $\lambda_R = m$ a running solution is born out of the diffusive state by the tangent mechanism described earlier. The intermittent behavior of the system consists of long segments of correlated iterates running to the right or to the left interspersed with chaotic motion. Thus, close to bifurcation a very simple representation of the diffusive motion is possible: Since the iterates in the basins consist of steps of roughly m cells (there is a slight drift in the m-unit displacement per iteration due to the motion across the resonance basin, but this is small compared to the hopping distance, which is at least one cell long) the actual velocity (not the velocity mod 1 discussed in Sec. III),

$$v_l = x_{l+1} - x_l = S(x_l;\lambda) - x_l , \qquad (4.5)$$

is apparently constant in the basins and is equal to

$\pm m$; the fraction of time spent in the watershed is small[16] $O(\epsilon^{1/2})$ and motion in the watershed simply serves to randomize the velocity, i.e., provides random entry into the right or left basins. A typical trajectory will therefore consist of long runs where the velocity is strongly correlated $(\simeq \pm m)$ interrupted by "collisions," which randomize the velocity.

The above description of the motion suggests a calculation of the diffusion coefficient based on the velocity autocorrelation function. Using Eq. (4.5), the expression for D in terms of the mean-square displacement may be written in the form

$$D = \lim_{n \to \infty} \frac{1}{2n} \sum_{l=0}^{n-1} \sum_{l'=0}^{n-1} \langle v_l v_{l'} \rangle$$
$$= \lim_{n \to \infty} \sum_{i=0}^{n-1} \langle v_i v_0 \rangle . \qquad (4.6a)$$

In the continuum model for the dynamics discussed in Sec. III, the maximum time that the velocity can remain correlated is t_{max}, the maximum length of time for passage through a resonance. Thus,

$$D = \int_0^{t_{max}} dt \langle v_t v_0 \rangle . \qquad (4.6b)$$

The diffusion coefficient and velocity autocorrelation function are now easily calculated from renewal theory[20] if we assume the duration of the velocity randomizing "collisions," i.e., time spent in the watershed, is negligible compared to the time spent in the basins, which will certainly be true close to bifurcation. Since collisions are assumed to completely randomize the velocity, it will remain correlated for a time t provided no collisions occur in this time interval. More specifically, the calculation proceeds as follows. The time series consists of segments of correlated iterates, with independently and identically distributed lengths, interrupted by collisions. Selecting an initial point at random, the probability that it falls on a segment with length between s and $s + ds$ is $\langle t \rangle^{-1} s P(s) ds$, where $P(s)$ is the probability of a run of length s given a random entry into a basin [Eq. (3.7)]. This expression is just the fractional length that all such segments occupy in the time series. The velocity will remain correlated during the time interval from $t = 0$ to t provided the right end point ("collision" vertex) of the segment with length s does not lie in this interval. Clearly segment lengths with values less than t must certainly occur in this interval. Given that we have selected a segment of length s the right collision vertex will have a rectangular distribution and therefore the probability that this end vertex, for $s \geq t$, does not lie in the interval of length t is

$1 - t/s$. Combining this conditional result with the above probability of selecting such a segment we have for the velocity correlation function

$$\langle v_t v_0 \rangle = \frac{m^2}{\langle t \rangle} \int_t^{t_{max}} ds \, (s - t) P(s) , \qquad (4.7)$$

which is m^2 times the average lapse before a collision. The diffusion coefficient is given by

$$D = \frac{\langle t^2 \rangle}{2 \langle t \rangle} m^2 . \qquad (4.8)$$

Using the expression for $P(t)$ given in Eq. (3.7), $\langle t^2 \rangle$ may be explicitly calculated for small ϵ with the result[22] $\langle t^2 \rangle \simeq 2 \langle t \rangle^2 \simeq (4m\epsilon)^{-1}$, and

$$D = \frac{m^{3/2}}{2\sqrt{2\epsilon}} . \qquad (4.9)$$

The diffusion coefficient is predicted to diverge as $\epsilon^{-1/2}$ as the running solution is approached; this is confirmed by the results in Fig. 13 and the data in Table II for the case $m = 1$.

C. Diffusion → chaotic running solutions

Although diffusive motion arises in this case by chaotic-band breakdown the diffusion-coefficient calculations is similar to that for the tangent mechanism. We described earlier how leaks develop in the chaotic bands as λ is increased above λ_{CR}. In the diffusive state near bifurcation iterates remain trapped in the chaotic bands for long periods of time since the escape probability per iteration, γ_R, is small. Although the local (mod-1) motion in the chaotic bands is irregular once an iterate is trapped
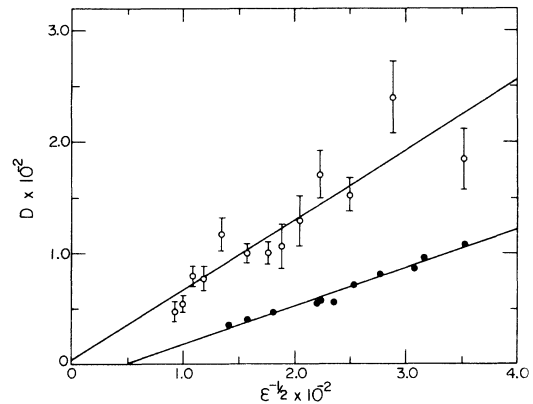
FIG. 13. Diffusion coefficient as a function of $\epsilon^{-1/2}$: Solid circles (●), periodic-running-solution region; open circles (O), chaotic-running-solution region.

it hops coherently to the right or left depending on the band which it enters. Again it is these long coherent runs that determine the value of the diffusion coefficient. We first compute the escape probability and then present the model for the diffusion coefficient.

The measure of the leaking region of a band can be calculated by considering Fig. 14, which shows a local (mod-1) representation of the dynamics; in this representation the equation of the bisectrix is $y = x + m$. Points lying in the interval $\mathcal{M} = (M_1, M_2)$ will escape. Referring to the figure the value of O_1 follows from the solution of the equation

$$\lambda \sin 2\pi O_1 = m , \qquad (4.10)$$

while O_2 can be found from

$$\lambda \sin 2\pi O_2 = O_1 - O_2 + m . \qquad (4.11)$$

To find M_1 and M_2 we need to calculate the intersections of the line VV', which has the equation $y = 1 + O_1 + (O_2 - O_1) = 1 + O_2$, with $S(x; \lambda)$. We have

$$S(M_1; \lambda) = m + O_2 . \qquad (4.12)$$

Near bifurcation these equations can be solved for $\mu(\mathcal{M}) = M_2 - M_1$,

$$\mu(\mathcal{M}) = 2 \left[\frac{\sin 2\pi M_B + \alpha}{2\pi^2 \lambda_{CR} \sin 2\pi M_B} \epsilon \right]^{1/2} , \qquad (4.13)$$

where

$$\alpha = \{ m + [S'(B_B; \lambda_{CR}) - 1](m + B_B - A_B) \} / \{ \lambda_{CR} S'(A_B; \lambda_{CR})[S'(B_B; \lambda_{CR}) - 1] \} \qquad (4.14)$$

and M_B, A_B, and B_B are the location of the maximum and its images under S and $S^{(2)}$ (mod 1) at the bifurcation value λ_{CR}. A similar calculation can be carried out for the chaotic solution running to the left.

The escape probability per iteration is given by

$$\gamma_R = \int_{\mathcal{M}} \rho(x) dx \simeq \rho(M_B) \mu(\mathcal{M}) , \qquad (4.15)$$

where the invariant density is normalized over a bandwidth. (The maximum at bifurcation is $M_B = 0.2729358383$.) Within a chaotic band the invariant density closely corresponds to that for the logistic equation $x_{t+1} = 4x_t(1 - x_t)$; $\rho(x) = [\pi \sqrt{x(1-x)}]^{-1}$,[11] and a direct estimate of γ_R (for $m = 1$) is possible, $\gamma_R = 1.214\epsilon^{1/2}$. Given
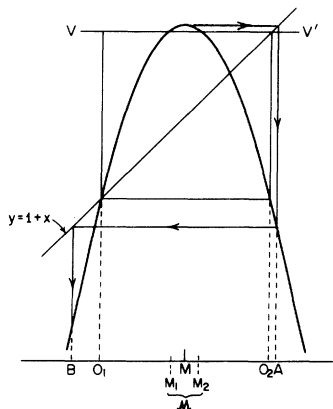
FIG. 14. A local (mod-1) representation of the dynamics for λ near λ_{CR} for $m = 1$. Local representation is achieved by iterating with respect to the shifted bisectrix $y = 1 + x$.

that the motion is chaotic within a band (mod 1) and the escape probability per iteration is small, the sojourn times in the chaotic bands will be exponentially distributed,[23]

$$P(t) = \gamma_R \exp(-\gamma_R t) . \qquad (4.16)$$

The average sojourn time is $\tau_{CR} = \gamma_R^{-1} \equiv \mathscr{C}_{CR} \epsilon^{1/2}$. For $m = 1$ Eq. (4.15) predicts $\mathscr{C}_{CR} = 0.823$ while the numerical computations give the result $\mathscr{C}_{CR} = 0.781$.

The picture of the escape dynamics near bifurcation is just a Poisson process: There are long runs of iterates to the right or left with velocity $\pm m$ (there is, of course, a small dispersion about this value due to the chaotic motion in a band) interrupted by collisions, i.e., entry into the watershed followed by re-entry into a band. Since an iterate can be reinjected into either right- or left-running chaotic bands once it enters the watershed, collisions serve to randomize the velocity just as in the tangent case. Given that the lengths of segments of correlated iterates are exponentially distributed, we may select the initial time $t = 0$ in the velocity correlation function to correspond to an entry into a chaotic band.[20] The velocity correlation function is again related to the probability that no collision occurs in the time t, which is now given by

$$\langle v_t v_0 \rangle = m^2 \int_t^\infty ds \, P(s) , \qquad (4.17)$$

and the diffusion coefficient is

$$D = m^2 \tau_{CR} = \frac{m^2}{\gamma_R} = m^2 \mathscr{C}_{CR} \epsilon^{-1/2} . \qquad (4.18)$$

We again have the prediction that D should diverge as $\epsilon^{-1/2}$, which is born out in the results of Table II and Fig. 13.

D. Diffusion → confined period 2

The mechanism by which period 2 is born out of a diffusive state by a tangent bifurcation process was described in Secs. II and III. Because of the intermittent character of the chaotic motion near a tangent bifurcation the dependence of the diffusion coefficient on the parameter distance from bifurcation can be obtained by arguments which are analogous to those given earlier for the transition from diffusion to running solutions. However, now the "laminar" part of the motion is confined and does not contribute to the diffusion coefficient; also the intertwined character of the period-2 orbits leads to a more complicated description of the diffusive dynamics.

The results in Fig. 12 indicate that the diffusion coefficient vanishes as $\epsilon^{1/2}$ near bifurcation; the origin of this dependence is easily explained on the basis of the intermittency picture presented earlier. Close to the bifurcation point the time series will consist of long segments of period-2-like motion where the iterates are confined to basins, interspersed with small segments in the watersheds where the motion is diffusionlike. From the analysis in Sec. III the average length of time spent in a period-2 resonance grows as $\epsilon^{-1/2}$ ($\tau_t = \mathscr{C}_t \epsilon^{-1/2}$) (Ref. 24) while the average length of time of a chaotic burst in the watershed $\tau'_{\mathscr{W}}$ is presumed to be independent of ϵ. [One may estimate that $\tau'_{\mathscr{W}} \simeq 7.13$ (Ref. 25)]. Hence, the fraction of the iterates which contribute to the diffusive motion is

$$f'_{\mathscr{W}} = \tau'_{\mathscr{W}}/(\tau_t + \tau'_{\mathscr{W}}) \simeq \frac{\tau'_{\mathscr{W}}}{\mathscr{C}_t} \epsilon^{1/2} \ ,$$

and the diffusion coefficient is

$$D = f'_{\mathscr{W}} D'_{\mathscr{W}} \ , \tag{4.19}$$

where $D'_{\mathscr{W}}$ is the diffusion coefficient which characterizes the dynamics in the watershed. The details of the entries into the various watersheds from the basins (cf. Sec. III B) and the subsequent dynamics in the watershed are somewhat involved. For example, $\mathscr{W}_2^{(i)}$ can be entered from $\mathscr{B}_2^{(i+1)}$ and $\mathscr{B}_1^{(i)}$ while $\mathscr{W}_1^{(i)}$ cannot be entered directly from a basin. If one ignores such details relating to the initial correla-

tions of iterates in the watershed and simply assumes motion in the watershed is random and characterized by a mean step length $l \simeq \lambda_t/2$, a crude estimate of $D'_{\mathscr{W}}$ is possible: $D'_{\mathscr{W}} \simeq l^2/2 \simeq \lambda_t^2/8$. Thus,

$$D \simeq \frac{\tau'_{\mathscr{W}} \lambda_t^2}{8 \mathscr{C}_t} \epsilon^{1/2} \ . \tag{4.20}$$

The $\epsilon^{1/2}$ behavior of D is verified by the results in Fig. 12 while data in Table II show that the crude estimate of the prefactor given above is in rough accord with the numerical result.

E. Diffusion → chaotic period 2

The description of the transition from diffusive motion to the confined period-2 chaotic bands occurs by chaotic-band breakdown and the diffusion-coefficient calculation closely parallels that of the previous subsection. Since the probability of escape from a band is small for values of λ slightly above λ_{Ct} the time series consists of long segments of iterates confined to the chaotic bands interspersed with runs of iterates which lie in the regions between the bands; motion in this region also appears to be chaotic.

Given this description of the dynamics, a rough calculation of the diffusion coefficient is easily carried out. Those iterates which lie in the chaotic bands will not contribute to the mean-square displacement or diffusion coefficient. Thus, we again expect the overall diffusion coefficient to be given by the product of the fraction of time spent in the watershed $f_{\mathscr{W}}^{Ct}$ times the diffusion coefficient which characterizes the motion in the watershed $D_{\mathscr{W}}^{Ct}$; $D = f_{\mathscr{W}}^{Ct} D_{\mathscr{W}}^{Ct}$. If $\tau_{\mathscr{W}}^{Ct}$ is the average length of a diffusive period in the watershed and τ_{Ct} is the average length of a confined period in the chaotic band, then, as earlier, $f_{\mathscr{W}}^{Ct} = \tau_{\mathscr{W}}^{Ct}/(\tau_{\mathscr{W}}^{Ct} + \tau_{Ct})$. Now, however, the calculation of τ_{Ct} follows from considerations similar to those given for the running chaotic-band case and depends on the probability of escape per iteration from the chaotic period-2 bands γ_t.

The escape probability per iteration γ_t can be computed by referring to Fig. 15. From this figure one can see that iterates which fall in the region $\mathscr{M}$ will "leak out" of the chaotic band. The local description of iteration is given most conveniently by writing the equation of the bisectrix as $y = m + 1 - x$ as in Fig. 15. The equations deter-

mining the points O_1 and O_2 in this figure are

$$S(O_2;\lambda)=m+1-O_2$$

and

$$O_1=A_B+\frac{\left[\dfrac{(m+1-2B_B)}{1+S'(B_B;\lambda_{Ct})}-(m+1-A_B-B_B)\right]}{\lambda_{Ct}S'(A_B;\lambda_{Ct})}\epsilon\equiv A_B+\alpha_t\epsilon$$

and

$$O_2=B_B-\frac{\epsilon\sin2\pi B_B}{1+S'(B_B;\lambda_{Ct})}\ .$$

The points M_1 and M_2 are determined by the intersection of the line VV' with the map function:

$$\mu(\mathcal{M})=M_2-M_1=2\left[\frac{\sin2\pi M_B+\alpha_t}{2\pi^2\lambda_{Ct}\sin2\pi M_B}\epsilon\right]^{1/2}\ .$$

$$(4.23)$$

The probability of escape per iteration from the chaotic period-2 bands is given by

$$\gamma_t=\int_{\mathcal{M}}\rho(x)dx\simeq\mu(\mathcal{M})\rho(M_B)\ ,\qquad(4.24)$$

where the density is normalized to unity in a band. For $m=1$ we find $(M_B=0.266\,457\,38)$ $\gamma_t=1.425\epsilon^{1/2}$. Thus, the average lifetime in the chaotic period-2 bands is obtained from arguments such as those in Sec. IV C and is $\tau_{Ct}=1/\gamma_t=\mathscr{C}_{Ct}\epsilon^{-1/2}$. Equation (4.24) yields $\mathscr{C}_{Ct}=0.702$ while direct computation gives $\mathscr{C}_{Ct}=0.663$. Since $\tau_{Ct}\sim O(\epsilon^{-1/2})$, $f_{\mathcal{W}}^{Ct}\sim O(\epsilon^{1/2})$ and the diffusion coefficient is predicted to vanish as $\epsilon^{1/2}$,

$$D=\frac{\tau_{\mathcal{W}}^{Ct}l^2}{2\mathscr{C}_{Ct}}\epsilon^{1/2}\simeq\frac{\tau_{\mathcal{W}}^{Ct}\lambda_{Ct}^2}{8\mathscr{C}_{Ct}}\epsilon^{1/2}\ ,\qquad(4.25)$$

where the last two equalities follow by assuming a simple random-walk model with steps of length $l\simeq\lambda_{Ct}/2$ in the watershed. The lifetime $\tau_{\mathcal{W}}^{Ct}$ may be roughly estimated as in Ref. 25 and one finds $\tau_{\mathcal{W}}^{Ct}\simeq3.73$, while direct numerical calculations yields $\tau_{\mathcal{W}}^{Ct}\simeq11$. As the data in Table II and Fig. 12 show this simple model provides a good approximation to the numerical results.

In all five cases considered above there is strong numerical evidence for the predicted $\epsilon^{\pm1/2}$ behavior. In addition, the prefactors of $\epsilon^{\pm1/2}$ are also adequately given by the rather crude dynamical models. More elaborate models of the diffusive dynamics can be constructed, especially for the last

$$S(O_1;\lambda)=m+1-O_2\ .\qquad(4.21)$$

Close to bifurcation O_1 and O_2 can be found by a perturbation calculation about their transition values, A_B and B_B, respectively. We find

$$(4.22)$$

two cases reported in Table II, but we have not attempted to do this.

V. DISCUSSION

Because of the simple structure of the climbing-sine map, a rather detailed discussion of the bifurcation patterns and description of the diffusion process could be given. The results indicate that diffusive motion arises through several mechanisms for this translationally invariant system: For all mechanisms the diffusion coefficient depends on ϵ, the parameter distance from bifurcation, as $\epsilon^{1/2}$ or $\epsilon^{-1/2}$, arising from the smooth quadratic character of the map, and the dynamics in the various parameter regions can be distinguished by the characteristic features of the time series from which the mean-square displacement is constructed.

We have noted in the Introduction that this study was motivated by the observed dynamics of systems with periodic forces that possess translational symmetry. Our one-dimensional-map model was not derived from the differential flows of Eq. (1.1) or (1.2) so the general applicability of some of our conclusions needs further testing. It is clear that the
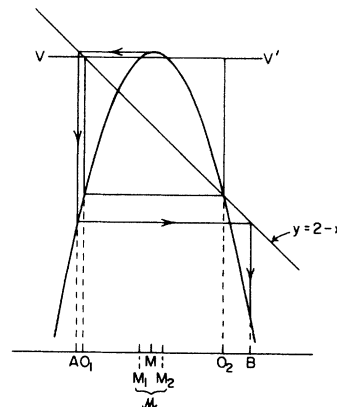
FIG. 15. A local description of map iterates used in the estimate of the size of the leaking region. In this representation map iterations are carried out with reference to the bisectrix $y=2-x$.

map model exhibits all of the expected types of behavior: confined, running, and diffusive solutions. Other features, e.g., the intermittent character of the diffusive motion preceding the appearance of running solutions, are also in accord with the map's behavior. However, there has been no work, to our knowledge, on quantitative aspects of the diffusive state in these systems, such as the calculation of diffusion coefficients and a study of their behavior as the differential flow parameters are varied. The computational difficulty associated with such calculations was one motivation for our one-dimensional-map study. It would be interesting to see to what extent the map predictions for the diffusion coefficient near the bifurcation points apply to differential flows and real systems.

After this paper was prepared we became aware of recent related work by Geisel and Nierwetberg[26] that considers the chaotic-band-merging transition to diffusion, with and without noise, for one-dimensional maps with translational symmetry.

ACKNOWLEDGMENT

[1]See, for example, *Physics of Superionic Conductors*, edited by M. B. Salamon (Springer, New York, 1979); B. A. Huberman and J. P. Crutchfield, Phys. Rev. Lett. 43, 1743 (1979). In the latter study the full periodic potential is not employed.

[2]B. A. Huberman, J. P. Crutchfield, and N. H. Packard, Appl. Phys. Lett. 37, 750 (1980).

[3]R. W. Leven and B. P. Koch, Phys. Lett. 86A, 71 (1981).

[4]M. Levi, F. C. Hoppensteadt, and W. L. Miranker, Q. Appl. Math. 36, 167 (1978).

[5]From Eq. (2.5) the sum of the components of such a period 2, $\{x, x'\}$ say, is n since $x' = S(x; \lambda)$. The center (mean) of the orbit is therefore $n/2$. If n is even this is a cell boundary and if n is odd a cell midpoint. The graph of S is *antisymmetric* about such points, since rotation by π leaves it invariant. Thus rotation about the center $n/2$ exchanges x and x' and we call such period 2's *symmetric*.

[6]The critical parameter value λ_M for migration between cells is smaller than $\frac{3}{4}$. Since S is periodic it is sufficient to consider the maximum in the first cell [0,1). Migration begins when this maximum touches $y = 1 = S(x; \lambda)$. But we have $S(\frac{1}{4}; \frac{3}{4}) = 1$, and $S'(\frac{1}{4}; \frac{3}{4}) \neq 0$ so that there is a point $x \in [0,1)$ such that $S(x; \frac{3}{4}) > 1$ and (a suitable neighborhood of) this point will be mapped into [1,2). The calculation of the precise value of λ_M is given in Sec. III.

[7]R. M. May, Nature 261, 459 (1976).

[8]P. Collet and J. -P. Eckmann, *Iterated Maps on the Interval as Dynamical Systems* (Birkhäuser, Basel, 1980).

[9]R. M. May, Ann. N. Y. Acad. Sci. 316, 517 (1979).

[10]M. J. Feigenbaum, J. Stat. Phys. 19, 25 (1978); 21, 669 (1979).

[11]S. Grossmann and S. Thomae, Z. Naturforsch. 32a, 1353 (1977).

[12]S. -J. Chang and J. Wright, Phys. Rev. A 23, 1419 (1981).

[13]E. N. Lorenz, Ann. N. Y. Acad. Sci. 357, 282 (1980).

[14]B. A. Huberman and J. Rudnick, Phys. Rev. Lett. 45, 154 (1980).

[15]Y. Pomeau and P. Manneville, in *Intrinsic Stochasticity in Plasmas*, edited by G. Laval and D. Gresillon (Editions de Physique, Orsay, 1979); Commun. Math. Phys. 74, 189 (1980).

[16]S. Fraser and R. Kapral, Phys. Rev. A 23, 3303 (1981); 25, 2827 (1982).

[17]J. E. Hirsch, B. A. Huberman, and D. J. Scalapino, Phys. Rev. A 25, 519 (1982).

[18]G. Mayer-Kress and H. Haken, Phys. Lett. 82A, 151 (1981).

[19]J. -P. Eckmann, L. Thomas, and P. Wittwer, J. Phys. A 14, 3153 (1981).

[20]See, for example, D. R. Cox and H. D. Miller, *The Theory of Stochastic Processes* (Chapman and Hall, London, 1972).

[21]S. J. Shenker and L. P. Kadanoff, J. Phys. A 14, L23 (1981).

[22]The small ϵ corrections to this result are $O(\sqrt{\epsilon})$ and $O(\sqrt{\epsilon} \ln \epsilon)$.

[23]Exponential distribution of lifetimes was also found by J. A. Yorke and E. D. Yorke, J. Stat. Phys. 21, 263 (1979) in a study of transient chaos in the Lorenz model. R. Shaw, Z. Naturforsch. 36a, 80 (1981), has observed that the first passage time to a small target is similarly distributed for chaotic motion.

[24]The average length of time spent in a basin in the stroboscopic representation of Sec. III is $\langle t \rangle = \pi/2C\eta = (4\pi\sqrt{2\lambda_t}\sin2\pi\xi_1^B)^{-1}\epsilon^{-1/2}$. The average length of time spent in a period-2 resonance is twice this value:

$$\tau_t = 2\langle t \rangle = (2\pi\sqrt{2\lambda_t}\sin2\pi\xi_1^B)^{-1}\epsilon^{-1/2}$$

$$\equiv \mathscr{C}_t\epsilon^{-1/2} \simeq 0.299\epsilon^{-1/2} .$$

[25]One may also roughly estimate $\tau'_{\mathscr{W}}$ by assuming that the capture probability per iteration κ is given by the measure of the basins in the unit interval and that the capture process is a Bernoulli trial. The measure of a

basin is $\mu(\mathscr{B}_2^{(i)})=\mu(\mathscr{B}_1^{(i)})=4(\xi_1^B-M_B)\simeq0.07$. Since there are two basins in each cell $\kappa\simeq2\mu(\mathscr{B}_1^{(i)})\simeq0.14$. The average lifetime is $\tau_{\mathscr{W}}^t=\kappa^{-1}\simeq7$. The measured value is $\tau_{\mathscr{W}}^t\simeq12$. As in the case of the logistic equation

there is evidently transient correlated motion in $\mathscr{W}$ (see Ref. 16).

[26]T. Geisel and J. Nierwetberg, Phys. Lett. **48**, 7 (1982).